

Evidence for neutron star triaxial free precession in Her X-1 from *Fermi*/GBM pulse period measurements

Dmitry Kolesnikov,^{1*} Nikolai Shakura¹ and Konstantin Postnov^{1,2}

¹*Moscow State University, Sternberg Astronomical Institute, Universitetskij pr. 13, 119234 Moscow, Russia*

²*Kazan Federal University, Kremlyovskaya 18, 420008 Kazan, Russia*

Accepted XXX. Received YYY; in original form ZZZ

ABSTRACT

Her X-1/HZ Her is one of the best studied accreting X-ray pulsars. In addition to the pulsating and orbital periods, the X-ray and optical light curves of the source exhibit an almost periodic 35-day variability caused by a precessing accretion disk. The nature of the observed long-term stability of the 35-day cycle has been debatable. The X-ray pulse frequency of Her X-1 measured by the *Fermi*/GBM demonstrates periodical variations with X-ray flux at the Main-on state of the source. We explain the observed periodic sub-microsecond pulse frequency changes by the free precession of a triaxial neutron star with parameters previously inferred from an independent analysis of the X-ray pulse evolution over the 35-day cycle. In the *Fermi*/GBM data, we identified several time intervals with a duration of half a year or longer where the neutron star precession period describing the pulse frequency variations does not change. We found that the NS precession period varies within one per cent in different intervals. Such variations in the free precession period on a year time scale can be explained by $\lesssim 1\%$ changes in the fractional difference between the triaxial neutron star's moments of inertia due to the accreted mass readjustment or variable internal coupling of the neutron star crust with the core.

Key words: X-rays: binaries – X-rays: individual: Her X-1 – stars: neutron

1 INTRODUCTION

Her X-1 is an accreting X-ray pulsar with a pulse period of $P^* = 1.24$ s around the optical star HZ Her with an orbital period of 1.7 days (Tananbaum et al. 1972; Cherepashchuk et al. 1972). The binary system is viewed almost edge-on. This causes different eclipsing features, including periodic orbital eclipses by the optical star and X-ray dips due to gas streams shielding the line of sight (e.g., Shakura et al. 1999). The source also demonstrates a long-term 35-day X-ray flux modulation (Giacconi et al. 1973). It consists of an X-ray bright Main-on state lasting about seven binary orbital periods, followed by a first low state with an almost zero flux (about four orbits), a Short-on state less prominent than the Main-on (about four orbits), and a second low-on state (about four orbits), see Shakura et al. (1998a); Leahy & Wang (2020) for more detail.

The nature of the 35-day modulation has been debatable. One of the first explanation involved a freely precessing neutron star (NS) Brecher (1972); Novikov (1973). For the observed 35-day period to be the NS free precession period P_{pr} , an axially symmetric NS should maintain a tiny ellipticity of the order of $\Delta I/I \sim P^*/P_{\text{pr}} \sim 10^{-6}$ (here ΔI is the difference in the NS's moments of inertia). In the case of a single NS, the unavoidable internal dissipation would tend to secularly align the spin and precession axes. This argument has been considered disfavoring the NS free precession as the reason for the long-term periodicity in pulsars (e.g., Shaham (1977)). The precession of an accretion disk around NS provides another explanation

to the 35-day cycle (e.g., Katz 1973; Roberts 1974; Petterson 1975, and subsequent papers). Presently, a rich phenomenology, both in the X-ray and optical, supports the presence of a tilted, retrograde, precessing accretion disk in Her X-1 (e.g., Boynton et al. 1973; Leahy 2003; Klochkov et al. 2006; Brumback et al. 2021). In the middle of the Main-on and Short-on states, the disk is maximum open to the observer's view, while during the low states, the outer parts of the tilted disk block the X-ray source.

Extensive X-ray observations of Her X-1 demonstrate that there can occur long (with a duration of up to 1.5 years) anomalous low states of the X-ray source during which the X-ray flux is completely extinguished but the X-ray irradiation of the optical star HZ Her persists (Parmar et al. 1985; Vrtilek et al. 1994; Coburn et al. 2000; Boyd et al. 2004; Still & Boyd 2004). These anomalous low states are likely due to vanishing the disk tilt to the orbital plane. As long as the disk tilt is close to zero, the X-ray source remains blocked from the observer's view by the disk's outer parts. An analysis of archive optical observations of HZ Her using photo plates showed that in the past there were periods when the X-ray irradiation effect was absent altogether (Jones et al. 1973; Hudec & Wenzel 1976). This means that sometimes in Her X-1/HZ Her binary system, the accretion onto the neutron star can cease completely (Bisnovatyi-Kogan et al. 1978). The cessation of accretion could occur, for example, because of a sudden jump in the NS magnetic field, which sometimes are observed in Her X-1 (Staubert et al. 2019), or a decrease in the mass inflow from the optical star, which can turn-off accretion due to the propeller effect.

The fact that the 35-day cycle re-appears in phase with the av-

* E-mail: kolesnikovkda@gmail.com

erage 35-day ephemeris after the end of anomalous low states and the stable periodic behavior of X-ray pulse profiles [Staubert et al. \(2013\)](#) requires a ‘stable clock’ mechanism operating in Her X-1/HZ Her ([Staubert et al. 2009](#)), which may be the NS free precession. Indeed, a model of two-axial NS free precession can reproduce the observed regular X-ray pulse profile changes with the 35-day phase ([Postnov et al. 2013](#)). This model involves a complex non-dipole magnetic field structure near the surface of accreting NS in Her X-1 and pencil-beam local emitting diagram. The non-dipole surface fields includes an additional quadrupole component producing ring-like structures around the NS magnetic poles ([Shakura et al. 1991](#)). This additional field doesn’t distort the NS’s form which is assumed to be shaped by a much stronger internal magnetic field $\sim 10^{14}$ G ([Braithwaite 2009](#)). The model also can explain the complicated optical variability of HZ Her over the 35-day cycle, which is primarily shaped by the irradiation effect of the optical star’s atmosphere by the X-ray emission from NS ([Kolesnikov et al. 2020](#)). A triaxial NS precession in Her X-1 was proposed earlier by us ([Shakura et al. 1998b](#)) to explain an anomalously narrow 35-day cycle of Her X-1 observed by HEAO-1. Presently, there is a growing empirical evidence that NS free precession could be responsible for different long-term periodicities in single magnetized NS, such as magnetars and fast radio bursts (FRBs) (see, e.g. [Levin et al. 2020](#); [Zanazzi & Lai 2020](#); [Cordes et al. 2021](#); [Wasserman et al. 2021](#); [Makishima et al. 2021](#)).

A precessing, pulsating NS should exhibit regular pulse period (or frequency) variations with a fractional amplitude change of $\Delta P^*/P^* \approx P^*/P_{\text{pr}} \sim 10^{-6}$ (e.g. [Ruderman 1970](#); [Truemper et al. 1986](#); [Bisnovatyj-Kogan et al. 1989](#); [Bisnovatyj-Kogan & Kahabka 1993](#); [Shakura 1995](#)). This tiny pulse frequency variations of Her X-1 can be searched for by the continuous monitoring of X-ray sources.

In this paper, we show that the periodic sub-microsecond pulse period variability observed in Her X-1 at the 35-day cycle maxima (the Main-on state) by *Fermi*/GBM (Gamma-ray Burst Monitor) ([Meegan et al. 2009](#)) can be explained by the motion of X-ray emitting region on the NS surface during the free precession of a triaxial NS. A preliminary analysis of the *Fermi*/GBM data for the two-axial NS free precession was reported in [Shakura et al. \(2021\)](#).

2 FERMI/GBM X-RAY PULSAR HER X-1 FREQUENCY MEASUREMENTS

Fermi/GBM X-ray pulsar Her X-1 frequency measurements are publicly available¹ and updated on daily basis. The measured frequency $\nu(t)$ of Her X-1 can be represented as a sum of non-periodic long-term frequency variability $\nu_0(t)$ and periodic 35-day frequency variability $\delta\nu(t)$:

$$\nu(t) = \nu_0(t) + \delta\nu(t) \quad (1)$$

or, equivalently, in terms of the angular frequency:

$$\Omega(t) = \Omega_0(t) + \delta\Omega(t). \quad (2)$$

In accreting pulsars like Her X-1, the long-term pulsar frequency trend $\Omega_0(t)$ can be due to changing accretion torques, see [Fig. 2](#).

Assuming that the pulsating flux is emitted near the north magnetic pole N of a rotating solid body, the 35-day periodic variations $\delta\Omega(t)$ are defined by the rate of change of the angle Φ of the spherical

triangle $I_3\Omega N$, see [Fig. 1](#):

$$\delta\Omega(t) = \frac{d\Phi(t)}{dt}. \quad (3)$$

Here we show that the periodic change of the angle Φ with parameters as in Her X-1 can be explained by a freely precessing NS. We start with considering a two-axial NS precession, which can be treated analytically, and continue with a more general case of triaxial NS free precession.

3 FREE PRECESSION OF THE NEUTRON STAR

3.1 Precession of an axially symmetric NS

It is straightforward to calculate analytically the pulse frequency variations from a freely precessing axially symmetric NS when the NS moments of inertia $I_1 = I_2 \neq I_3$ (see, e.g. [Ruderman 1970](#); [Truemper et al. 1986](#); [Bisnovatyj-Kogan et al. 1989](#); [Bisnovatyj-Kogan & Kahabka 1993](#); [Shakura 1995](#)). Below we will assume that the precession frequency is much lower than the spin frequency of the NS so that the total angular momentum vector to a high accuracy coincides with the NS spin vector. When the NS spin frequency vector Ω is misaligned with the principal inertia axis I_3 by angle γ , the free precession angular frequency reads

$$\omega = \Omega \frac{I_1 - I_3}{I_1} \cos \gamma. \quad (4)$$

The observed pulse frequency is modulated by the time derivative of the angle Φ marking the NS precession phase (see [Fig. 1](#)). For the angle β between the north magnetic pole N and I_3 axis, the phase Φ can be found from the sine and cosine theorem for spherical triangles:

$$\cos \Phi(t) = \frac{\sin \beta \sin \varphi(t)}{\sqrt{1 - [\cos \gamma \cos \beta + \sin \gamma \sin \beta \cos \varphi(t)]^2}}, \quad (5)$$

where $\varphi(t)$ is the azimuthal angle of the vector Ω in a rigid coordinate frame related to the NS’s principal inertia axes (the light grey lines in [Fig. 1](#)). In the course of NS free precession, $\varphi(t)$ is a linear function of time:

$$\varphi(t) = \varphi_0 + \Omega t. \quad (6)$$

The amplitude of the periodic sub-microsecond pulse frequency periodic variations observed by *Fermi*/GBM in Her X-1 can be easily adjusted by assuming a two-axial NS free precession with the appropriate choice of the NS ellipticity $\Delta I/I$ ([Shakura et al. 2021](#)). However, the shape of the measured pulse frequency variations as a function of the 35-day phase can be better reproduced by assuming a slight NS triaxiality, $I_1 \neq I_2 \neq I_3$.

3.2 Precession of a triaxial NS

Given the moments of inertia $I_1 < I_2 < I_3$ and angular velocity Ω , the NS rotational energy is

$$2E = I_1\Omega_1^2 + I_2\Omega_2^2 + I_3\Omega_3^2, \quad (7)$$

and the angular momentum is

$$M^2 = I_1^2\Omega_1^2 + I_2^2\Omega_2^2 + I_3^2\Omega_3^2. \quad (8)$$

¹ <https://gammaray.nsstc.nasa.gov/gbm/science/pulsars/lightcurves/herx1.html>

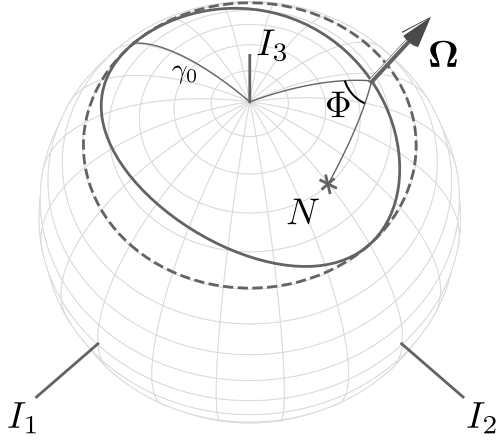


Figure 1. A schematic view of free precession of a triaxial neutron star. The surface coordinates (light grey lines) are related to NS inertial axes I_1 , I_2 , I_3 . The path of the NS angular momentum vector (the spin axis) on the NS surface Ω during the triaxial free precession is shown by the solid line. The path of Ω during a two-axial free precession is shown by the dashed line. The asterisk marks the north magnetic pole N . Φ is the phase angle of the north magnetic pole N .

Following Landau & Lifshitz (1976), the motion of the angular momentum vector is described by the equations

$$\Omega_1 = \sqrt{\frac{2EI_3 - M^2}{I_1(I_3 - I_1)}} \operatorname{cn}\tau \quad (9)$$

$$\Omega_2 = \sqrt{\frac{2EI_3 - M^2}{I_2(I_3 - I_2)}} \operatorname{sn}\tau \quad (10)$$

$$\Omega_3 = \sqrt{\frac{M^2 - 2EI_1}{I_3(I_3 - I_1)}} \operatorname{dn}\tau, \quad (11)$$

where $\operatorname{cn}\tau$, $\operatorname{sn}\tau$, $\operatorname{dn}\tau$ are elliptic Jacobi functions, and the dimensionless time τ is

$$\tau = t \sqrt{\frac{(I_3 - I_2)(M^2 - 2EI_1)}{I_1 I_2 I_3}}. \quad (12)$$

The free precession period reads

$$P = 4 \sqrt{\frac{I_1 I_2 I_3}{(I_3 - I_2)(M^2 - 2EI_1)}} \int_0^{\pi/2} \frac{du}{\sqrt{1 - k^2 \sin^2 u}}, \quad (13)$$

where the parameter k is defined as

$$k^2 = \frac{(I_2 - I_1)(2EI_3 - M^2)}{(I_3 - I_2)(M^2 - 2EI_1)}. \quad (14)$$

For a given NS rotational period, the fractional moment inertia differences $\Delta I_2 = (I_2 - I_1)/I_1$ and $\Delta I_3 = (I_3 - I_1)/I_1$ fully determine the NS free precession period P . However, a realistic NS is not a fully rigid body. In Her X-1, the NS free precession period can change due to the action of external torques, mass accretion, non-rigid coupling between the crust and the core, etc.

In the *Fermi*/GBM data, we identified 10 time intervals ΔT_k , $k = \text{I}, \dots, \text{X}$ comprising $\sim 5 - 20$ consecutive cycles that can be described by approximately constant P_k (see below Fig. 3 and Table 2). (Due to scarce points in some cycles, the data chunks ΔT_k with constant 35-day cycle duration are not always contingent and can be separated by time intervals, which we excluded from the analysis;

their inclusion does not change the results but worsens the χ^2 of the fit). We assigned equal values of ΔI_2 for all 35-day cycles to minimize residuals between the model and observations. The parameter $(\Delta I_3)_k$ was calculated individually from Eq. (13) inside each data intervals ΔT_k with constant period P_k . Thus, inside each data interval, for given NS parameters and free precession period P_k we can numerically calculate positions of the vector Ω , the phase angle Φ (see Fig. 1) and derivative $d\Phi/dt$ defining the pulse frequency variations.

4 MODELLING OF HER X-1 PULSAR FREQUENCY VARIATIONS

In accreting X-ray pulsars, the long-term pulse frequency variations $\nu_0(t)$ are caused by various factors, e.g. by variable accretion torque which are difficult to predict. Here, in order to subtract the long-term pulse frequency variations, we model $\nu_0(t)$ as a cubic spline passing through nodes τ_j , $\nu_0(\tau_j)$ as follows.

We introduce the residuals R between the observed pulsar frequency measurements ν_i at moments t_i and the theoretical model $\nu(t)$:

$$R = \sum_i (\nu(t_i) - \nu_i)^2. \quad (15)$$

where the index i runs through all frequency measurements, index j corresponds to the 35-day cycles considered, see Table A1 in Appendix A. Our theoretical model $\nu(t)$ is the sum of the periodic 35-day pulsar frequency variations $d\Phi/dt$ due to the NS free precession and long-term trend $\nu_0(t)$:

$$\nu(t) = \frac{1}{2\pi} \frac{d\Phi(t)}{dt} + \nu_0(t) \quad (16)$$

The time coordinate τ_j of the spline nodes is defined as the mean time of the pulse frequency measurement within the j -th Main-on:

$$\tau_j = \frac{1}{N_j} \sum_i t_i, \quad (17)$$

Here, N_j is the number of observations within the j -th Main-on. The spline value $\nu_0(\tau_j)$ is the difference between the mean pulse frequency and the model NS free precession frequency at the moment τ_j :

$$\nu_0(\tau_j) = \frac{1}{N_j} \sum_i \nu_i - \frac{1}{2\pi} \frac{d\Phi(\tau_j)}{dt}, \quad (18)$$

Parameters of the long-term evolution $\nu_0(t)$ and 35-day variations of X-ray pulse frequency $\delta\nu(t)$ were evaluated by minimizing the residuals R , equation 15. Parameters of the triaxial NS free precession are listed in Tables 1 and 2. The minimizing of the residuals R were done using the LMFIT package (Newville et al. 2014).

Inside each k -th data interval with constant 35-day cycle duration P_k , the fractional NS moment of inertia difference ΔI_3 was optimized to fit the observed pulse frequency variations measured by *Fermi*/GBM. The parameters ΔI_2 and the NS principal axis of inertia I_3 misalignment with the angular momentum γ_0 were fixed for all 35-day cycles.

The trajectory of the NS angular momentum Ω on the surface (see Fig. 1) can be defined by ΔI_2 , ΔI_3 and the misalignment angle γ_0 at the NS precession zero phase (cf. Eq. (4) for two-axial case, where this angle is constant). With fixed ΔI_2 and γ_0 , the NS free precession period P_k (Eq. 13) is defined by ΔI_3 only. As seen from Table 2, the 35-day period in Her X-1 changes within the range

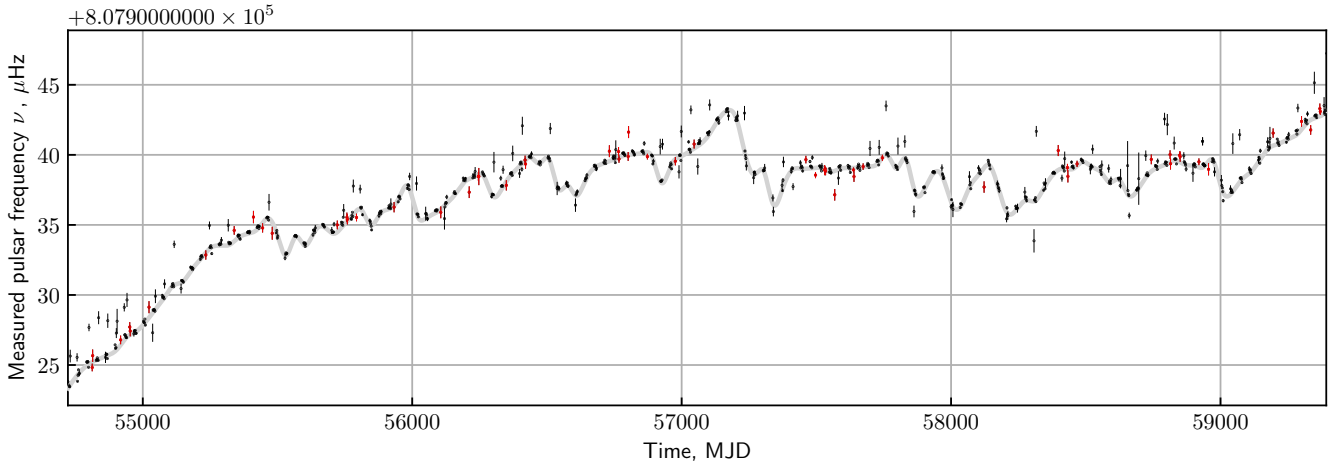


Figure 2. Her X-1 pulse frequency as a function of time. The dots show *Fermi*/GBM measurements (in black during the 35-day cycle Main-on phases 0.0–0.35, in red otherwise). The grey solid line shows the long-term pulse frequency variations $\nu_0(t)$ approximated as described in Section 4.

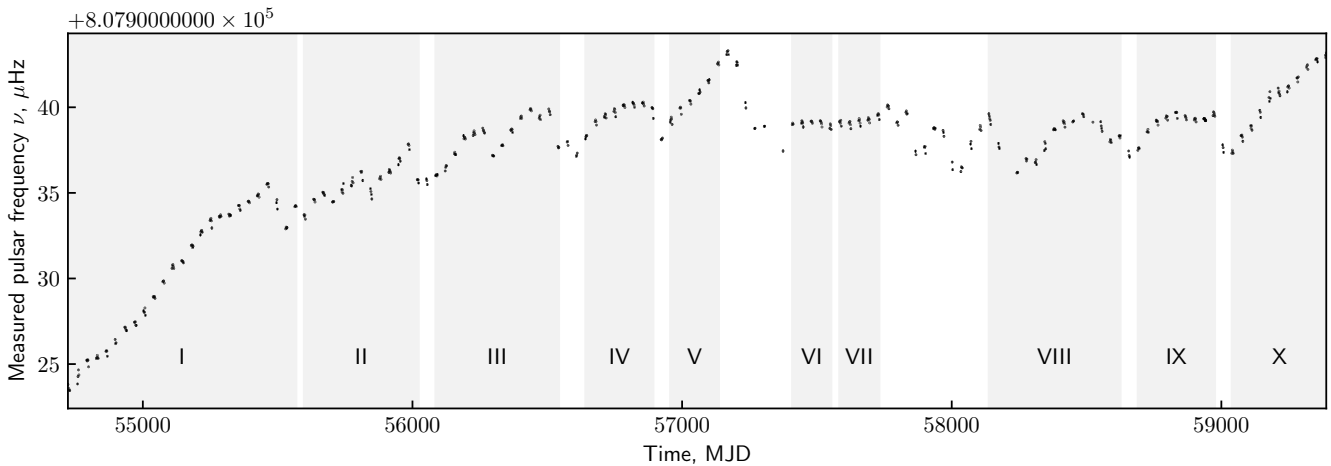


Figure 3. The same as in Fig. 2 with grey zones showing intervals ΔT_k with constant NS free precession period P_k (see Table 2). Also, measurements with error larger than $0.1\mu\text{Hz}$ or outside Main-on state were removed.

$34^d.8 - 35^d.2$, i.e. $|\Delta P/P| \approx 1\%$ on a timescale of half a year or longer. Variations of the moments of inertia are possible for a not fully rigid NS body; variations of the misalignment between the NS principal inertia axis I_3 and angular momentum can be due to the internal coupling between the NS crust and core. Both cases are physically plausible for a realistic NS. In our model with fixed γ_0 , the changes in NS moments of inertia can be due to the redistribution of mass accreted onto the NS. Indeed, on a year timescale, the accreted mass in Her X-1 is $\delta M \sim 10^{17} [\text{g/s}] \times 3 \times 10^7 [\text{s}] \sim 3 \times 10^{24} \text{ g}$, i.e. the fractional change in the NS moment of inertia is $\delta I/I \approx \delta M/M \sim 10^{-9}$. Thus, the mass redistribution in the non-rigid NS body with a mean ellipticity of 10^{-6} could be sufficient to produce $\lesssim 1\%$ variations in the relative difference of the NS moments of inertia (see Table 2).

The NS free precession period P as a function of ΔI_3 in our model for Her X-1 with parameters from Table 1 is shown in Fig. 4. It is seen that a 1% variations in ΔI_3 alter the free precession period P correspondingly. Therefore, the NS free precession model

for Her X-1 suggests a 1% change in the NS body parameters on a year timescale. Similar indications have been obtained earlier from the analysis of O-C behaviour of the mean 35-day cycle duration (Postnov et al. 2013).

The best-fit modeling of the periodic X-ray pulse variations of Her X-1 by the triaxial NS free precession with parameters from Table 1 and Table 2 is shown in Figs. 5 and 6. The solid black line presents the model $\nu(t)$, with the 35-day cycle duration P_k adjusted using the fractional moment inertia difference ΔI_3 and the NS free precession zero phase at the beginning of each data interval ΔT_k listed in Table 2.

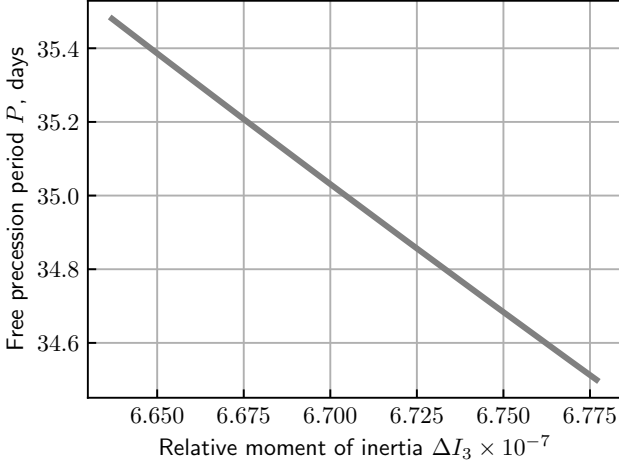


Figure 4. Triaxial NS free precession period P as a function of relative moment of inertia difference ΔI_3 with other parameters fixed, see Table 1.

Table 1. Triaxial free precession model parameters fixed during the fitting inside k -th data intervals with constant 35-day cycle duration P_k

Parameter	Symbol	Value
Ω and I_3 axis misalignment at zero free precession phase	γ_0	50°
Coordinates of the magnetic pole N	N_ϕ N_θ	90° 30°
Fractional moment inertia difference $(I_2 - I_1)/I_1$	ΔI_2	3×10^{-7}

5 DISCUSSION & CONCLUSION

The 0.3–0.5 microsecond variability of the X-ray pulse period of Her X-1 measured by *Fermi*/GBM² with ~ 0.1 microsec accuracy suggests the emitting region radial velocity amplitude $V_r/c \leq \Delta P^*/P^* = \Delta v^*/v^* \sim 3 \times 10^{-7}$. In the present paper, we have shown that such variations are possible for a freely precessing, likely triaxial NS in Her X-1. In the *Fermi*/GBM data, we have identified several time intervals with a duration of half a year or longer (see Fig. 3 and Table 2) where the NS precession period does not change noticeably. The NS precession period varies within 1% in different intervals. Such variations can be explained by $\lesssim 1\%$ changes in the NS moment inertia difference due to accreted mass readjustment or variable internal coupling of the NS crust with the core.

In principle, besides the NS free precession, the pulsar frequency variations could be generated by the reflection from the warped accretion disk precessing with the angular velocity Ω_d . In that case, the maximum radial velocity of the reflector should be $V_{r,max} = \Omega_d R_{in} \approx 2 \times 10^2$ cm/s for the assumed inner disk radius $R_{in} \approx 10^8$ cm. This velocity would give rise to the Doppler frequency modulation with an amplitude of $\Delta v_{ref}/v^* \sim 10^{-8}$, much smaller than the observed value. The Doppler broadening of the reprocessed pulsations on the accretion disk flow would smear the precession-induced frequency variations. There is another point of

concern with the disk reflection model. In Her X-1, the beginning of the 35-day cycle is known to be due to the central X-ray source opening by the outer parts of the precessing accretion disk (Kuster et al. 2005). If the pulse period variations were produced by the reflection from the disk, one would expect correlation between the 35-day cycle beginning and the pulse frequency maximum, which is not found. Therefore, the possibility that the observed pulsar period change in Her X-1 is due to reprocessing of the X-ray pulses on the disk seems unlikely.

In our model, the inner part of the disk should align with the NS’s equator due to magnetic forces (Lipunov & Shakura 1980; Lipunov et al. 1981; Lai 1999) during the 35-day cycle Main-on. The pulsar period 1.24 s should be close to the equilibrium value (the magnetospheric radius is close to the corotation radius), suggesting the inner disk radius $\sim 100 R_{ns}$. Therefore, the accreting plasma gets frozen into the magnetic field and is canalised onto the NS’s surface in regions defined by the local magnetic field structure. In this case, the precession of the outer parts of the disk should not produce variations of the hot spot geometry.

During the Short-on stage, the X-ray flux from Her X-1 is several times as low as at the Main-on, and the pulse period determination from *Fermi*/GBM data is less certain. However, on several occasions (e.g., on MJD 54952, 55757, 56418, 57532) the pulse period is found to be at the approximately the same level as at the Main-on². In our model, the Short-on pulse is shaped by emitting arcs located symmetrically to the inertia axis I_3 but phase-separated by π (see Fig. 2 and 3 in Postnov et al. 2013). Therefore, the expected pattern of the pulse profile variations during the Short-on should be similar to the Main-on. Future accurate measurements of the X-ray pulse timing in Her X-1 Short-on are valuable to test this prediction.

We conclude that a freely precessing NS in Her X-1 with parameters inferred from an independent analysis of X-ray pulse profile evolution with 35-day phase (Postnov et al. 2013) can explain regular sub-microsecond pulse period changes observed by *Fermi*/GBM. To explain a $\lesssim 1\%$ variations in the NS free precession period on a year timescale, the model requires the corresponding change in the NS parameters (relative difference in the moments of inertia or the NS angular momentum misalignment with the principal moment of inertia). These changes might be related to the variable internal coupling of the NS crust with the core. The model has also proved successful in explaining the HZ Her optical light curves over the 35-day cycle as well (Kolesnikov et al. 2020). Therefore, after about half century of studies, the NS free precession as the inner clock mechanism for the observed 35-day cycle in Her X-1/HZ Her is further supported by the X-ray pulse period frequency variations observed by *Fermi*/GBM.

ACKNOWLEDGEMENTS

We thank the anonymous referee for useful comments. The work of DK and NS was supported by the RSF grant 21-12-00141 (modelling of Her X-1 pulsar frequency variations; calculation of *Swift*/BAT 35-day cycle turn-on times). The authors acknowledge the Interdisciplinary Scientific Educational School of Moscow University ‘Fundamental and applied space research’. KP acknowledges support by the Kazan Federal University Strategic Academic Leadership Program (“PRIORITY-2030”).

² <https://gammaray.nsstc.nasa.gov/gbm/science/pulsars/lightcurves/herx1.html>

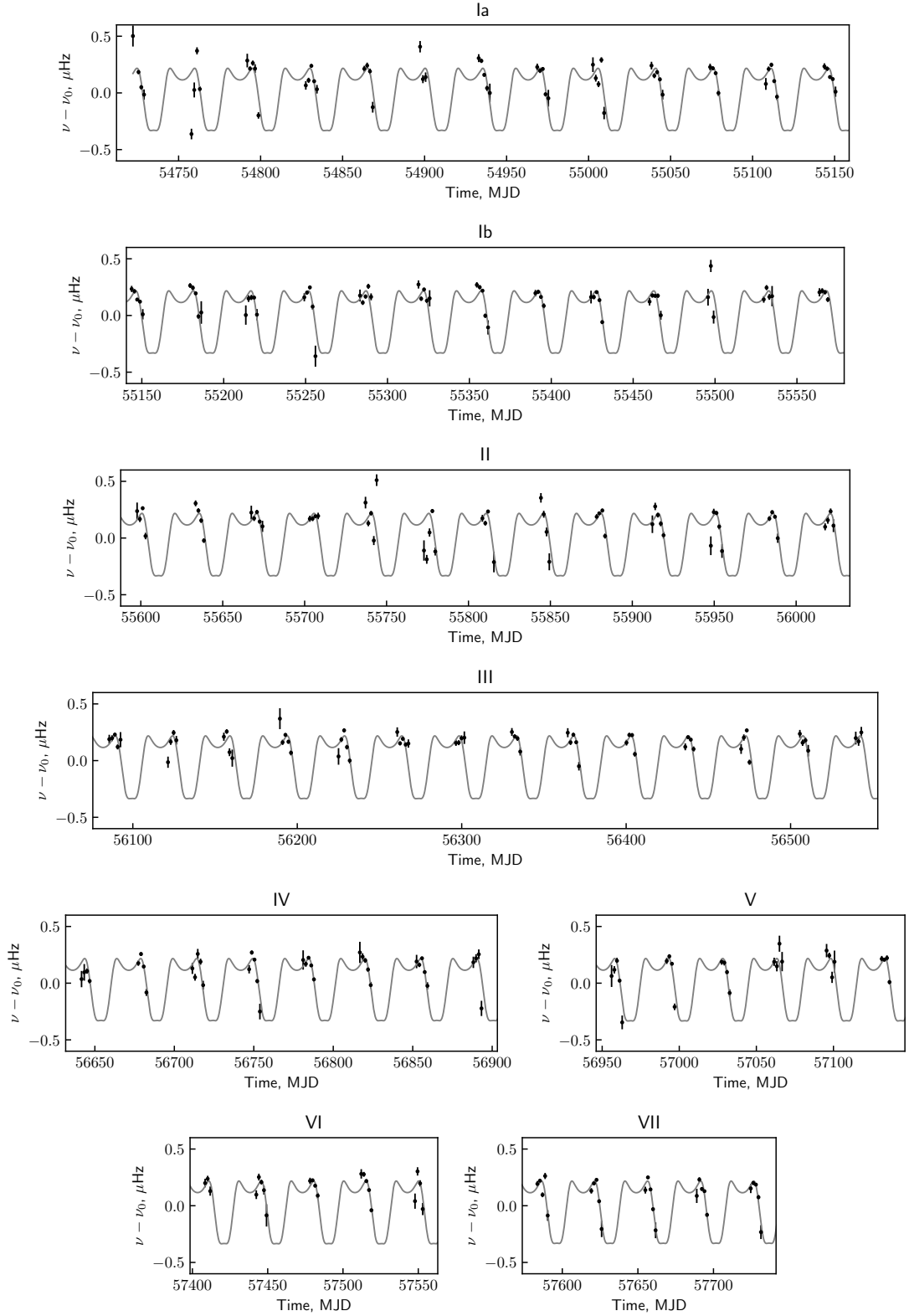
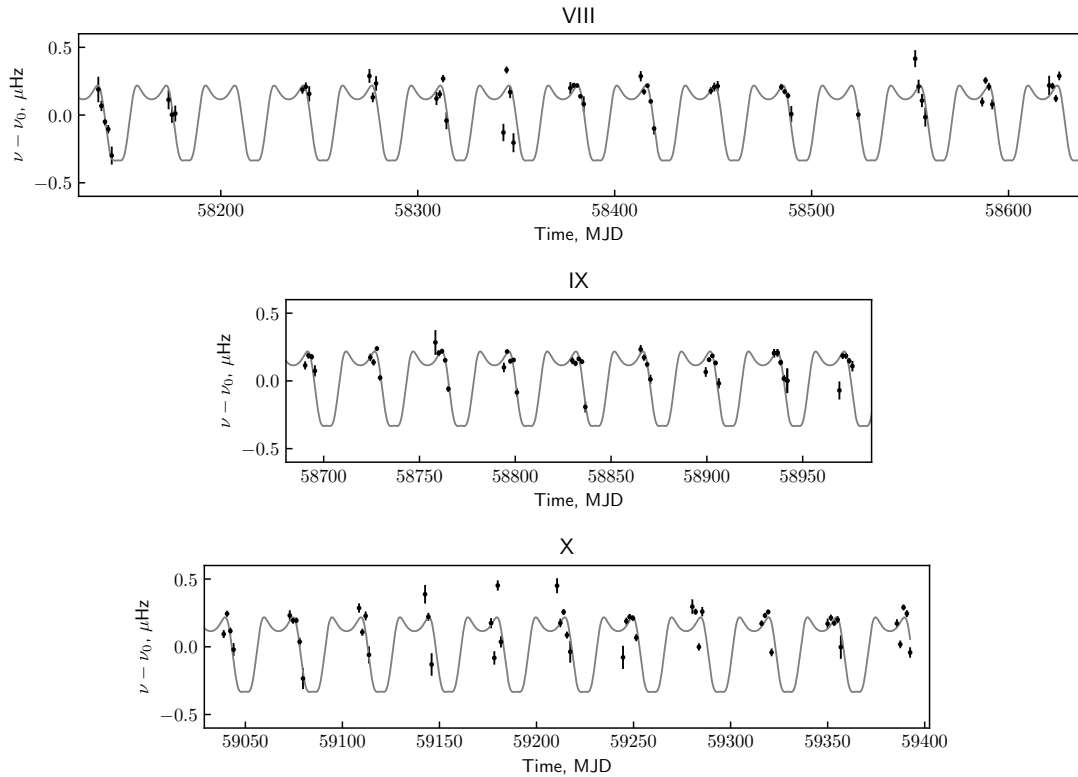


Figure 5. The best-fit modeling (the solid line) of the periodic X-ray pulse frequency variations of Her X-1 by the triaxial NS free precession (intervals I–VII from Table 2). The dots show the *Fermi*/GBM X-ray pulse frequency measurements.

Table 2. Triaxial NS free precession model parameters inside k -th data intervals with constant 35-day cycle duration P_k marked in Fig. 3.

Interval number k	ΔT_k , MJD	Cycle duration, P_k	$\Delta I_3 \times 10^{-7}$	φ_0^*	Reduced χ^2
I	54722.15 – 55568.84	35.14	6.68	−0.45	7.2
II	55597.73 – 56022.78	35.02	6.70	−0.305	9.3
III	56085.66 – 56543.01	34.85	6.73	0.024	4.9
IV	56641.62 – 56893.27	35.25	6.67	−1.13	3.2
V	56956.11 – 57136.34	35.05	6.70	−0.63	4.4
VI	57408.42 – 57552.93	34.83	6.73	0.01	1.8
VII	57583.53 – 57731.39	35.1	6.69	−0.88	4.8
VIII	58137.80 – 58625.74	34.8	6.73	−0.01	4.4
IX	58690.33 – 58975.96	35.01	6.70	0.0	3.6
X	59039.85 – 59392.50	35.0	6.70	−0.015	10.0

* initial phase φ_0 (see Eq. 6) is calculated for the time of first *Fermi*/GBM data point for Her X-1 $t_0 = \text{MJD } 54722.15470$


Figure 6. The same as in Fig. 5 for intervals VIII–X from Table 2.

DATA AVAILABILITY

The data underlying this article are available in the article, *Fermi*/GBM X-ray data are freely available at <https://gammaray.nsstc.nasa.gov/gbm/science/pulsars/lightcurves/herx1.html>, *Swift*/BAT X-ray data are freely available at <https://swift.gsfc.nasa.gov/results/transients/HerX-1/>.

REFERENCES

- Bisnovatyi-Kogan G. S., Bochkarev N. G., Karitskaia E. A., Cherepashchuk A. M., Shakura N. I., 1978, *Soviet Astronomy Letters*, **4**, 43
 Bisnovatyi-Kogan G. S., Mersov G. A., Shefer E. K., 1989, *A&A*, **221**, L7
 Bisnovatyi-Kogan G. S., Kahabka P., 1993, *A&A*, **267**, L43
 Boyd P., Still M., Corbet R., 2004, *The Astronomer’s Telegram*, **307**, 1
 Boynton P. E., Canterna R., Crosa L., Deeter J., Gerend D., 1973, *ApJ*, **186**, 617
 Braithwaite J., 2009, *MNRAS*, **397**, 763
 Brecher K., 1972, *Nature*, **239**, 325
 Brumback M. C., Hickox R. C., Fürst F. S., Pottschmidt K., Tomsick J. A., Wilms J., Staubert R., Vrtilik S., 2021, *ApJ*, **909**, 186
 Cherepashchuk A. M., Efremov Y. N., Kurochkin N. E., Shakura N. I., Sunyaev R. A., 1972, *Information Bulletin on Variable Stars*, **720**
 Coburn W., et al., 2000, *ApJ*, **543**, 351
 Cordes J. M., Wasserman I., Chatterjee S., Batra G., 2021, arXiv e-prints, p. [arXiv:2107.12874](https://arxiv.org/abs/2107.12874)
 Giacconi R., Gursky H., Kellogg E., Levinson R., Schreier E., Tananbaum H., 1973, *ApJ*, **184**, 227
 Hudec R., Wenzel W., 1976, *Bulletin of the Astronomical Institutes of Czechoslovakia*, **27**, 325
 Jones C. A., Forman W., Liller W., 1973, *ApJ*, **182**, L109

Katz J. I., 1973, *Nature Physical Science*, **246**, 87

Klochkov D. K., Shakura N. I., Postnov K. A., Staubert R., Wilms J., Ketsaris N. A., 2006, *Astronomy Letters*, **32**, 804

Kolesnikov D. A., et al., 2020, *MNRAS*, **499**, 1747

Kuster M., Wilms J., Staubert R., Heindl W. A., Rothschild R. E., Shakura N. I., Postnov K. A., 2005, *A&A*, **443**, 753

Lai D., 1999, *ApJ*, **524**, 1030

Landau L. D., Lifshitz E. M., 1976, in Landau L., Lifshitz E., eds., *Mechanics* (Third Edition), third edition edn, Butterworth-Heinemann, Oxford, pp 96–130, doi:<https://doi.org/10.1016/B978-0-08-050347-9.50011-3>

Leahy D. A., 2003, *MNRAS*, **342**, 446

Leahy D., Wang Y., 2020, *ApJ*, **902**, 146

Levin Y., Beloborodov A. M., Bransgrove A., 2020, *ApJ*, **895**, L30

Lipunov V. M., Shakura N. I., 1980, *Soviet Astronomy Letters*, **6**, 14

Lipunov V. M., Semenov E. S., Shakura N. I., 1981, *Azh*, **58**, 765

Makishima K., Tamba T., Aizawa Y., Odaka H., Yoneda H., Enoto T., Suzuki H., 2021, arXiv e-prints, p. [arXiv:2109.11150](https://arxiv.org/abs/2109.11150)

Meegan C., et al., 2009, *ApJ*, **702**, 791

Newville M., Stensitzki T., Allen D. B., Ingargiola A., 2014, LMFIT: Non-Linear Least-Square Minimization and Curve-Fitting for Python, doi:[10.5281/zenodo.11813](https://doi.org/10.5281/zenodo.11813), <https://doi.org/10.5281/zenodo.11813>

Novikov I. D., 1973, *Soviet Ast.*, **17**, 295

Parmar A. N., Pietsch W., McKechnie S., White N. E., Truemper J., Voges W., Barr P., 1985, *Nature*, **313**, 119

Pettersson J. A., 1975, *ApJ*, **201**, L61

Postnov K., Shakura N., Staubert R., Kochetkova A., Klochkov D., Wilms J., 2013, *MNRAS*, **435**, 1147

Roberts W. J., 1974, *ApJ*, **187**, 575

Ruderman M., 1970, *Nature*, **225**, 838

Shaham J., 1977, *ApJ*, **214**, 251

Shakura N. I., 1995, HER X-1/HZ Her: 35-day Cycle, Freely Precessing Neutron Star and Accompanying Effects. Nova Science Publishers, p. 55

Shakura N. I., Postnov K. A., Prokhorov M. E., 1991, *Soviet Astronomy Letters*, **17**, 339

Shakura N. I., Ketsaris N. A., Prokhorov M. E., Postnov K. A., 1998a, *MNRAS*, **300**, 992

Shakura N. I., Postnov K. A., Prokhorov M. E., 1998b, *A&A*, **331**, L37

Shakura N. I., Prokhorov M. E., Postnov K. A., Ketsaris N. A., 1999, *A&A*, **348**, 917

Shakura N. I., Kolesnikov D. A., Postnov K. A., 2021, *Astronomy Reports*, **65**, 1039

Staubert R., Bezler M., Kendziorra E., 1983, *A&A*, **117**, 215

Staubert R., Klochkov D., Postnov K., Shakura N., Wilms J., Rothschild R. E., 2009, *A&A*, **494**, 1025

Staubert R., Klochkov D., Vasco D., Postnov K., Shakura N., Wilms J., Rothschild R. E., 2013, *A&A*, **550**, A110

Staubert R., et al., 2019, *A&A*, **622**, A61

Still M., Boyd P., 2004, *ApJ*, **606**, L135

Tananbaum H., Gursky H., Kellogg E. M., Levinson R., Schreier E., Giacconi R., 1972, *ApJ*, **174**, L143

Truemper J., Kahabka P., Oegelman H., Pietsch W., Voges W., 1986, *ApJ*, **300**, L63

Vrtilek S. D., et al., 1994, *ApJ*, **436**, L9

Wasserman I., Cordes J. M., Chatterjee S., Batra G., 2021, arXiv e-prints, p. [arXiv:2107.12911](https://arxiv.org/abs/2107.12911)

Zanazzi J. J., Lai D., 2020, *ApJ*, **892**, L15

Table A1. Pulse frequency long-term evolution

Cycle number j	τ_j MJD	$\nu_0(\tau_j) \times 10^{-5} + 0.8079$, Hz
383	54726.91	2.3476
385	54760.36	2.4355
386	54796.05	2.5070
387	54831.80	2.5380
388	54865.80	2.5659
389	54900.66	2.6082
390	54936.37	2.6978
391	54971.21	2.7340
392	55006.07	2.8031
393	55041.76	2.8834
394	55076.63	2.9694
395	55112.33	3.0662
396	55146.33	3.0910
397	55182.04	3.1806
398	55216.88	3.2679
399	55251.74	3.3362
400	55287.45	3.3517
401	55321.46	3.3598
402	55357.15	3.4129
403	55392.85	3.4379
404	55428.56	3.4796
405	55464.27	3.5462
406	55498.27	3.4341
407	55531.43	3.2819
408	55567.13	3.4153
409	55601.13	3.3524
410	55635.97	3.4482

APPENDIX A: HER X-1 LONG-TERM PULSE FREQUENCY EVOLUTION

Here we present the table of the spline values $\tau_j, \nu_0(\tau_j)$ of the long-term evolution of Her X-1 pulse frequency. The method of calculation of $\tau_j, \nu_0(\tau_j)$ is described in Section 4. The numbering of 35-day cycles follows the convention introduced by Staubert et al. (1983).

Table A1 – continued Pulse frequency long-term evolution

Cycle number j	τ_j MJD	$\nu_0(\tau_j) \times 10^{-5} + 0.8079$, Hz
411	55670.85	3.4878
412	55705.68	3.4367
413	55741.39	3.4997
414	55777.10	3.5698
415	55810.62	3.6085
416	55845.94	3.4974
417	55880.79	3.5782
418	55916.50	3.6168
419	55951.36	3.6936
420	55986.21	3.7729
421	56019.37	3.5627
422	56053.36	3.5510
422	56089.08	3.5909
424	56123.93	3.6445
425	56157.93	3.7143
426	56193.66	3.8105
427	56229.34	3.8463
428	56264.19	3.8520
429	56299.04	3.7043
430	56333.04	3.7663
431	56368.75	3.8619
432	56403.61	3.9323
433	56438.46	3.9829
434	56473.31	3.9383
435	56508.17	3.9673
436	56541.32	3.7576
437	56575.32	3.7831
438	56609.32	3.7088
439	56645.02	3.8269
440	56679.87	3.9120
441	56714.75	3.9438
442	56750.44	3.9712
443	56785.31	3.9958
444	56821.00	4.0038
445	56856.69	4.0148
446	56891.56	3.9804
447	56924.70	3.7997
448	56959.57	3.9324
449	56994.40	3.9863
450	57030.10	4.0276
451	57064.13	4.0673
452	57099.84	4.1381
453	57133.83	4.2445
454	57169.52	4.3165
455	57204.38	4.2516
456	57236.69	3.9947
457	57269.85	3.8602
458	57305.56	3.8793
459	57339.56	3.6466
460	57375.24	3.7617
461	57410.11	3.8909
462	57444.96	3.9009
463	57480.66	3.9054
464	57516.37	3.9028
465	57551.23	3.8788
466	57586.08	3.9012
467	57621.77	3.9046
468	57657.47	3.9111
469	57693.46	3.9164
470	57728.89	3.9432
471	57762.88	3.9992
472	57798.58	3.9025
473	57832.60	3.9695

Table A1 – continued Pulse frequency long-term evolution

Cycle number j	τ_j MJD	$\nu_0(\tau_j) \times 10^{-5} + 0.8079$, Hz
474	57865.75	3.7353
475	57900.60	3.7525
476	57935.46	3.8704
477	57969.45	3.8382
478	58003.45	3.6421
479	58036.61	3.6337
480	58070.63	3.7774
481	58105.48	3.8695
482	58141.17	3.9264
483	58175.18	3.7653
484	58208.36	3.5862
485	58243.18	3.6102
486	58277.18	3.6743
487	58312.04	3.6719
488	58346.89	3.7699
489	58380.89	3.8702
490	58416.61	3.9037
491	58450.59	3.8997
492	58486.31	3.9490
493	58521.13	3.9164
494	58556.02	3.8763
495	58589.17	3.8031
496	58624.88	3.8219
497	58658.09	3.7112
498	58692.78	3.7505
499	58726.88	3.8553
500	58762.58	3.9048
501	58797.45	3.9344
502	58832.30	3.9583
503	58868.00	3.9290
504	58902.00	3.9213
505	58937.69	3.9152
506	58973.42	3.9562
507	59006.56	3.7438
508	59041.41	3.7264
509	59075.41	3.8179
510	59110.27	3.8715
511	59144.27	3.9584
512	59179.14	4.0506
513	59213.98	4.0771
514	59248.84	4.1086
515	59283.68	4.1487
516	59318.54	4.2293
517	59352.54	4.2662
518	59389.16	4.3000